Research Square

Preprints are preliminary reports that have not undergone peer review.
They should not be considered conclusive, used to inform clinical practice,
or referenced by the media as validated information.

Single-Cell Genomic Profiling Identifies an H3F3B–SEPTIN6 Axis Associated with Malignant Epithelial Phenotypes in Lung Adenocarcinoma

Xianghua Zhou

xhZhou_haining@163.com

Affiliated Haining Hospital of Jiaxing University

Liqin Wu

Affiliated Haining Hospital of Jiaxing University

Fanfan Yang

Affiliated Haining Hospital of Jiaxing University

Chunxiao Hou

Affiliated Haining Hospital of Jiaxing University

Jiaqi Wang

Affiliated Haining Hospital of Jiaxing University

Research Article

Keywords: H3F3B, SEPTIN6, lung adenocarcinoma, single-cell RNA sequencing, malignant epithelial cells, tumor progression

Posted Date: November 1st, 2026

DOI: https://doi.org/10.21203/rs.3.rs-10963935/v1

License: This work is licensed under a Creative Commons Attribution 4.0 International License.
Read Full License

Additional Declarations: No competing interests reported.

Abstract

Background

Lung adenocarcinoma is an important cause of cancer morbidity and mortality among women, yet sex-specific molecular features of malignant epithelial populations remain incompletely understood. This study investigated the expression and functional significance of H3F3B and its association with SEPTIN6 in LUAD.

Methods

Single-cell RNA sequencing data from three publicly available lung datasets were integrated to characterize epithelial cell populations and identify genes associated with malignant phenotypes. Differential expression, pathway enrichment, protein–protein interaction, and gene co-expression analyses were performed to characterize H3F3B-associated transcriptional programs. H3F3B expression was further evaluated in three paired LUAD and adjacent tissue specimens by reverse transcription quantitative polymerase chain reaction, Western blotting, and immunohistochemistry. Functional effects of H3F3B were investigated in A549 cells using overexpression and siRNA-mediated knockdown, followed by proliferation, migration, and invasion assays. SEPTIN6 expression was assessed following H3F3B perturbation.

Results

Integration of 665,761 epithelial cells from 878 samples identified distinct epithelial populations, including a prominent Secretory Club/AT2-like malignant population. H3F3B was significantly upregulated in malignant epithelial cells and showed increased expression across LUAD stages. H3F3B expression was positively correlated with SEPTIN6 expression in the integrated dataset. In paired patient tissues, H3F3B expression was higher in LUAD tissues than in adjacent tissues at both the mRNA and protein levels. H3F3B overexpression increased A549 cell proliferation, migration, and invasion, whereas H3F3B knockdown produced the opposite effects. SEPTIN6 expression increased following H3F3B overexpression and decreased following H3F3B knockdown.

Conclusion

H3F3B is associated with malignant epithelial states in LUAD and promotes proliferative, migratory, and invasive phenotypes in A549 cells. Its positive association with SEPTIN6 and the concordant regulation of SEPTIN6 following H3F3B perturbation suggest that the H3F3B–SEPTIN6 pathway may contribute to LUAD progression. Further studies are required to define the molecular mechanism underlying this regulatory relationship and to establish its clinical relevance.

1. Introduction

Lung adenocarcinoma (LUAD) is a major subtype of non-small cell lung cancer and remains an important cause of cancer-related morbidity and mortality[1]. Despite advances in molecularly targeted therapy and immunotherapy, substantial interpatient and intratumoral heterogeneity continues to influence disease progression, treatment response, and clinical outcomes. This heterogeneity is particularly evident within malignant epithelial populations, which contain distinct cellular states associated with proliferation, differentiation, invasion, and therapeutic resistance. Single-cell RNA sequencing (scRNA-seq) provides an opportunity to resolve these cellular states and identify molecular programs that may be obscured in bulk transcriptomic analyses[2]. Large-scale single-cell studies have demonstrated substantial cellular diversity within lung cancer and have identified distinct malignant epithelial states associated with tumor progression and metastatic behavior. However, the molecular regulators that distinguish aggressive epithelial populations from non-malignant epithelial states remain incompletely characterized[3, 4]. However, many prior studies have focused broadly on the immune or stroma compartment or have limited resolution within epithelial tumor cells. For lung adenocarcinoma specifically, GSE131907 comprised 208,506 single cells from 58 LUAD specimens (including tumor, lymph node metastases, and matched normal tissues) and has illuminated lineage relationships and metastatic programs[5]. The expanding accumulation of scRNA-seq data necessitates robust integrative frameworks to harmonize batch effects, increase statistical power, and enable cross-cohort comparisons of rare transcriptomic states. At the same time, histone variant biology, and specifically the histone H3.3 family encoded by H3F3A and H3F3B, has emerged as a key regulatory axis in chromatin remodeling and gene expression control across development and disease[6]. While the role of H3F3A (H3.3-A) has been investigated in lung cancer its overexpression is reported to drive migration and metastasis via intronic regulatory element binding (in particular at GPR87) [7] the functional significance of H3F3B (H3.3-B) remains comparatively underexplored in lung adenocarcinoma. Given that H3F3B is a paralog differing by only a few amino acids from H3F3A, yet may exert distinct regulatory roles or interactomes, we hypothesized that H3F3B could modulate tumor cell phenotypes via subtype-specific regulatory networks.

Therefore, in this study, we present an Integrated Single-Cell Transcriptomic and Experimental Pipeline to systematically characterize H3F3B in lung adenocarcinoma. We integrate three major scRNA-seq cohorts spanning a total of 665,761 epithelial cells (from 878 samples), leveraging advanced batch correction (BBKNN) and pseudo-batch aggregation to preserve cell-state resolution and sample-level inference. We perform differential expression and pathway enrichment comparing tumor vs. normal states across 10 major epithelial clusters. We further construct co-expression and network models to define putative downstream effectors of H3F3B, refining candidate gene sets via a three-way intersection of cluster membership, expression change, and correlation strength ($|r| > 0.2$, FDR < 0.05) [8, 9]. To validate our computational findings and probe functional consequences, we deploy immunohistochemistry on patient tissues, and perturb H3F3B expression in A549 cells via plasmid overexpression and siRNA knockdown, followed by assays including RT–qPCR, Western blotting, proliferation (CCK-8), migration/invasion (Transwell/Matrigel)[10]. Through this tightly integrated

pipeline, we aim not only to map the transcriptional footprints of H3F3B in the epithelial tumor compartment, but also to experimentally validate how H3F3B modulation influences proliferative and invasive phenotypes. Our approach provides a quantitative, cross-cohort framework and a mechanistic basis for further exploring H3F3B as a potential biomarker or therapeutic axis in lung adenocarcinoma. To our knowledge, no previous study has integrated multi-cohort single-cell transcriptomics with functional validation to define the role of H3F3B in LUAD progression.

2. Method

2.1 Ethics statement and patient tissue collection

This study was conducted in accordance with the Helsinki Declaration and approved by the Ethics Committee of Affiliated Haining Hospital of Jiaxing University (Approval ID: T20260130-X). Three primary LUAD tissue specimens and paired adjacent non-tumor tissues were collected at Affiliated Haining Hospital of Jiaxing University between 2023, October 1 and 2024 Feb 28. Written informed consent for research and publication was obtained from all patients prior to sample collection.

2.2 Dataset integration and preprocessing

To examine epithelial cell heterogeneity in lung adenocarcinoma, we integrated three publicly available scRNA-seq datasets. The first, from Chan et al., 2021 (PMID: 34653364)[11], was accessed from CELLxGENE in January 2025 (https://cellxgene.cziscience.com/collections/62e8f058-9c37-48bc-9200-e767f318a8ec). The second, from Salcher et al., 2022 (PMID: 36368318)[3], was obtained from the European Genome–Phenome Archive in February 2025 (https://luca.icbi.at/). The third, from Sikkema et al., 2023 (PMID: 37291214)[12], was downloaded from CELLxGENE in March 2025 (https://cellxgene.cziscience.com/collections/6f6d381a- 7701-4781-935cdb10d30de293). Raw count matrices were processed using Scanpy v1.9.6. Cells with > 500 total counts, > 200 detected genes, and < 20% mitochondrial reads were retained; genes expressed in < 3 cells were removed. Metadata were harmonized by standardizing patient IDs, tissue type (tumor vs. adjacent), and barcoding formats. Cross-checks with original annotations ensured accurate cell labelling. After quality control and integration, the final dataset comprised 665,761 high-quality epithelial cells from 878 patient samples across clinical stages I–IV. This large, harmonized multi-cohort atlas provides a robust foundation for subsequent clustering, differential expression, and network analyses.

2.3 Single-Cell RNA Sequencing Data Analysis

Filtered data were normalized and log-transformed using Scanpy v1.9.6. Batch correction was performed using BBKNN (Batch-Balanced k-Nearest Neighbors) with n_pcs = 40, neighbors_within_batch = 3, trim = None, and annoy_n_trees = 10 [13]. Cell clustering was conducted with the Leiden algorithm at a resolution of 0.6 to resolve distinct epithelial subpopulations. Automated annotation was performed using CellTypist, employing lung-specific reference atlases. Annotation confidence was categorized into four levels (Very High, High, Medium, Low)[14]. To ensure statistical robustness, clusters were

aggregated into 878 pseudo-batches, each containing ≥ 30 cells and ≥ 10 expressed genes. A total of 10 major epithelial clusters were identified and subsequently analysed for differential gene expression and network connectivity.

2.4 Differential Expression and Network Analysis

Differential gene expression (DGE) analysis was conducted using edgeR v3.42.4 (Bioconductor, R), a widely used statistical package designed for analyzing RNA-seq count data based on negative binomial models[15]. Pseudo-batch aggregated count matrices were generated for each epithelial subtype, and a generalized linear model (GLM) framework was applied to assess differential expression between (i) tumor vs. adjacent normal tissues and (ii) tumor vs. control groups. The design matrix incorporated three covariates: sample identity, epithelial cell cluster, and disease state, to account for intra-sample heterogeneity and inter-cluster variability. To correct for batch effects introduced by combining multiple studies, ComBat [16] empirical Bayes adjustment was applied prior to model fitting. Differential expression testing employed quasi-likelihood F-tests within edgeR's GLM pipeline, which provides robust error control for overdispersed single-cell data. Statistical significance thresholds were set at false discovery rate (FDR) < 0.05, adjusted using the Benjamini–Hochberg procedure, and $|\log_2$ fold change$| \geq 0.5$ to focus on biologically meaningful transcriptional alterations. Genes meeting these criteria were considered significantly differentially expressed. This multi-level analytical framework enabled the detection of robust transcriptional changes across distinct epithelial subpopulations, while minimizing confounding effects from sample heterogeneity and inter-study variability. Differentially expressed genes (DEGs) were subjected to functional enrichment analysis using clusterProfiler v4.6.0[17] across multiple curated databases to comprehensively assess biological functions and pathways. Gene Ontology (GO) analysis included Biological Process, Molecular Function, and Cellular Component categories, highlighting terms such as cell proliferation (GO:0008283), chromatin remodeling (GO:0006338), and epithelial cell migration (GO:0010631). KEGG pathway enrichment identified relevant pathways including *PI3K-Akt* signaling (hsa04151), cell cycle (hsa04110), p53 signaling (hsa04115), and DNA replication (hsa03030). Reactome analysis captured curated modules such as chromatin organization (R-*HSA-4839726)*, cell cycle checkpoints (R-HSA-69620), and DNA repair (R-HSA-73894). Over-representation was evaluated using hypergeometric testing followed by FDR correction. We specifically interrogated pathways enriched in H3F3B-associated signatures, including WANG_TUMOR_INVASIVENESS, cell proliferation modules, and curated H3F3B protein–protein interaction networks. This allowed systematic assessment of pathways associated with tumor invasiveness, chromatin regulation, and proliferative signaling. Results were visualized through volcano plots, enrichment bar graphs, and pathway interaction networks to facilitate biological interpretation.

2.5 Gene Co-expression Network Analysis

H3F3B-centered co-expression analyses were performed using sample-level expression profiles. Pearson and Spearman correlation coefficients were calculated to evaluate relationships between H3F3B and other genes. Multiple testing was controlled using the false discovery rate. Genes were considered candidate H3F3B-associated genes based on significant correlation and differential

expression criteria. The top correlated genes were visualized using Cytoscape v3.9.1. Co-expression analyses were interpreted as associations and were not considered evidence of direct regulatory interactions.

2.6 In Vitro Functional Analyses

All in vitro experiments were performed using the human lung adenocarcinoma cell line A549.

2.6.1 Immunohistochemistry (IHC)

Formalin-fixed, paraffin-embedded lung tissue sections (4μm) were deparaffinized in xylene, rehydrated through graded ethanol series, and subjected to antigen retrieval using citrate buffer (pH 6.0) at 95°C for 20 minutes. Sections were blocked with 5% normal goat serum for 30 minutes at room temperature and incubated overnight at 4°C with anti-H3F3B primary antibody (Proteintech, 13754-1-AP) at a 1:200 dilution. Following washes with PBS, sections were incubated with HRP-conjugated secondary antibody (Vector Laboratories) for 1 hour at room temperature. Immunoreactivity was visualized using 3,3'-diaminobenzidine (DAB) chromogen and counterstained with hematoxylin. Slides were independently evaluated by two board-certified pathologists, blinded to clinical and experimental information. High-resolution images were acquired using a 3DHISTECH Pannoramic digital slide scanner (Budapest, Hungary), and quantitative analysis of staining intensity and distribution was performed using ImageJ v1.53 with color deconvolution.

2.6.2 Plasmid Construction and siRNA Transfection

he full-length H3F3B coding sequence was amplified and cloned into the pcDNA3.1 expression vector for H3F3B overexpression. H3F3B-targeting small interfering RNAs (siRNAs) were synthesized by RiboBio (Guangzhou, China). Transfection was performed using Lipofectamine 2000 (Thermo Fisher Scientific) according to the manufacturer’s instructions. Cells were harvested 48–72 h after transfection for subsequent analyses.

2.6.3 Quantitative Real-Time PCR (qPCR)

Total RNA was extracted from transfected A549 cells using TRIzol Reagent (Invitrogen, 15596026) according to the manufacturer’s protocol. RNA concentration and purity were assessed using a NanoDrop 2000 spectrophotometer (Thermo Fisher). cDNA synthesis was performed with EasyScript™ Reverse Transcriptase (TransGen Biotech, AE301-03) using 1 μg of total RNA per reaction. qPCR was carried out on an FTC-300 Real-Time Cycler (Funglyn Biotech Inc., Shanghai, China) using SYBR Green chemistry, with GAPDH serving as an internal reference. Each sample was run in triplicate, and relative gene expression was calculated using the $2^{-}\Delta\Delta Ct$ method, with non-transfected or scramble siRNA–transfected cells as controls.

2.6.4 Western Blotting

Total protein was extracted using RIPA buffer supplemented with protease and phosphatase inhibitors (Beyotime, P1005), and protein concentrations were determined using the BCA Protein Assay Kit (Beyotime, P0012). Equal amounts of protein (30–50 μg) were separated by 10% SDS–PAGE alongside a prestained protein molecular weight marker (ColorMixed Protein Marker 250, ABclonal, Cat. No. RM02949) and transferred to PVDF membranes (Millipore, IPVH00010). Membranes were blocked in 5% non-fat milk in TBST for 1 hour at room temperature, followed by incubation overnight at 4°C with primary antibodies: H3F3B (1:1000, Proteintech, 13754-1-AP), SEPTIN6 (1:1000, Proteintech, 12805-1-AP), and GAPDH (1:1000, Cell Signaling Technology, 5174S). After washing, membranes were incubated with HRP-conjugated secondary antibodies (Thermo Fisher) for 1 hour at room temperature. Protein bands were visualized using ECL chemiluminescence (Thermo Fisher, 32106) and quantified with ImageJ v1.53.

2.6.5 Cell Proliferation Assay (CCK-8)

Transfected A549 cells were seeded into 96-well plates at 5 × 10^3 cells/well in triplicate. Cell proliferation was monitored at 24, 48, 72, and 96 h using the CCK-8 assay. A549 cells were seeded at 5 × 10^3 cells/well in 96-well plates. At each time point, 10 μL of CCK-8 solution was added to each well and incubated for 2 h at 37°C. Absorbance was measured at 450 nm using a BioTek microplate reader. Growth curves were plotted to evaluate the effect of H3F3B knockdown or overexpression on cell proliferation.

2.6.7 Migration and Invasion Assays

Cell migration was evaluated using Transwell chambers (Costar, 3422), and invasion was assessed with Matrigel-coated inserts (Corning, 354480). 5 × 10^4 cells/well in serum-free medium were seeded in the upper chamber, and 600 μL of medium containing 20% FBS was added to the lower chamber as a chemoattractant. After 24 h incubation at 37°C in a 5% CO_2 incubator, cells remaining in the upper chamber were removed with a cotton swab. Migrated or invaded cells on the lower surface were fixed with 4% paraformaldehyde for 15 minutes, stained with 0.1% crystal violet for 30 minutes, rinsed, and air-dried. Images were captured under a bright-field microscope (Olympus, Japan) at five random fields per membrane, and the number of cells was quantified using ImageJ v1.53. Each experiment was performed in triplicate to ensure reproducibility.

2.7 Statistical Analysis

Statistical analyses were performed using GraphPad Prism v10.0. Continuous data are presented as mean ± standard deviation (SD). For comparisons between two independent groups, two-tailed Student's t-tests were used when the assumptions of normality and equal variance were satisfied; otherwise, the corresponding non-parametric test was applied. For paired comparisons of LUAD and adjacent tissue specimens, paired statistical tests were used. CCK-8 proliferation curves involving multiple time points were analyzed using two-way analysis of variance with appropriate multiple-comparison correction. For migration and invasion assays, comparisons between experimental groups were performed using two-tailed statistical tests as appropriate. $P < 0.05$ was considered statistically significant.

3. Results

3.1 Secretory Club/AT2-like cells are the primary malignant subpopulation of lung adenocarcinoma epithelial cells

To dissect the epithelial heterogeneity in lung adenocarcinoma (LUAD), we integrated three publicly available scRNA-seq datasets[3, 11, 12], comprising 665,761 epithelial cells from 878 patient-derived samples spanning clinical stages I–IV. After rigorous quality control, batch correction, and normalization, 9 distinct epithelial clusters were identified via Leiden clustering at resolution 0.6 (Fig. 1A). These included alveolar type 1 (AT1) cells, alveolar type 2 (AT2) cells, basal cells, ciliated cells, and malignant populations such as Secretory Club/AT2-like and Cycling Basal-like cells. Disease-state analysis revealed significant shifts in cell-type composition between non-cancer controls and lung cancer tissues (Fig. 1B). Malignant populations were restricted to tumor samples, with Secretory Club/AT2-like and Cycling Basal-like cells representing > 69% of epithelial cells in LUAD samples, with Secretory Club/AT2-like cells alone accounting for 47.6% **(Fig. 1CD)**. Marker gene analysis validated cluster identities: AT1 cells expressed AGER and PDPN, AT2 cells expressed SFTPC and SFTPA1, while Secretory Club/AT2-like cells specifically expressed LUAD-associated markers CEACAM6, SCGB3A2, and SPINK1 (Fig. 1E). Cycling Basal-like cells exhibited elevated MKI67 and BIRC5, indicating high proliferative potential.

3.2 Secretory Club/AT2-like cells exhibit significant transcriptional dysregulation in LUAD

UMAP-based dimensionality reduction of integrated scRNA-seq data revealed distinct segregation of Secretory Club/AT2-like cells from non-malignant epithelial populations, including AT1, AT2, basal, and ciliated cells, highlighting extensive transcriptional reprogramming associated with tumorigenesis (Fig. 2A). Differential gene expression analysis comparing tumor versus adjacent normal tissues identified a total of 1,418 significantly dysregulated genes (FDR < 0.01, $|\log_2 FC| > 1$), comprising 993 upregulated and 425 downregulated genes (Fig. 2B). Among the upregulated genes, H3F3B exhibited one of the highest fold changes, implicating it as a potential driver of malignant phenotypes. Functional enrichment analysis using Reactome revealed that upregulated gene programs in Secretory Club/AT2-like cells were highly enriched for pathways critical to tumor progression, including SemaA PAK-dependent axon repulsion, antigen processing and cross-presentation, interferon α/β signaling, platelet degranulation, and cell cycle checkpoint regulation (Fig. 2C). These results indicate that this malignant subpopulation concurrently engages immune evasion mechanisms, metabolic adaptation, and proliferative signaling, supporting a multifaceted role in LUAD pathobiology. Quantitative assessment of cell proportions confirmed that Secretory Club/AT2-like cells constituted approximately 42–50% of the malignant epithelial compartment, underscoring their dominant contribution to tumor-specific transcriptional landscapes.

3.3 H3F3B is a central hub gene in malignant epithelial cells

Analysis of H3F3B expression revealed robust upregulation across all LUAD stages, with statistically significant increases observed from early-stage tumors (stage I–II) to advanced-stage disease (stage III–IV; $p < 0.001$) (Fig. 3A). Single-cell network reconstruction identified H3F3B as a central hub gene, exhibiting extensive connectivity with histone variants (H4C3, H4C8, H4C11), chromatin remodeling factors, and cell cycle regulatory proteins (Fig. 3B). Secretory Club/AT2-like cells demonstrated the highest H3F3B-centered network activity, as quantified by integrated PPI scores, cell proliferation indices, and invasion metrics ($p < 0.001$; Fig. 3C–E). These data indicate that H3F3B not only functions as a transcriptional regulator of chromatin organization but also integrates proliferative and invasive signaling pathways within malignant epithelial subpopulations. Correlation network analysis revealed SEPTIN6 as the top non-histone gene associated with H3F3B (Spearman $r = 0.63$, FDR < 1e-72), suggesting the existence of a regulatory axis linking chromatin remodeling to cytokinesis and cytoskeletal organization (Fig. 3F). This interplay likely contributes to the enhanced proliferative and invasive potential observed in LUAD-specific malignant epithelial clusters, positioning H3F3B as a key mechanistic driver of tumor aggressiveness.

3.4 H3F3B is overexpressed in LUAD patient tissues

To validate transcriptomic findings, we examined tumor and adjacent normal tissues from three LUAD patients. RT-qPCR revealed a 4–6-fold increase in H3F3B mRNA in tumor tissues compared to NAT ($p < 0.01$; Fig. 4A). Western blot confirmed parallel protein-level upregulation (Fig. 4B). IHC analysis demonstrated strong nuclear H3F3B staining in tumor cells, with weak or absent staining in adjacent tissues (Fig. 4C–D). Quantitative image analysis revealed ~ 5.2-fold higher nuclear staining intensity in tumors, confirming H3F3B overexpression in patient-derived LUAD tissues.

3.5 H3F3B overexpression promotes LUAD cell proliferation, migration, and invasion

To elucidate the functional role of H3F3B in lung adenocarcinoma, we overexpressed H3F3B in the human LUAD cell line A549 using a pcDNA3.1-based expression construct. Quantitative real-time PCR and Western blotting confirmed robust upregulation of H3F3B mRNA and protein levels relative to vector-transfected controls (Fig. 5A–B). Functional assessment of cell proliferation using the CCK-8 assay revealed a significant increase in growth rates over four consecutive days in H3F3B-overexpressing cells compared to controls ($p < 0.01$; Fig. 5C). Specifically, absorbance measurements at 450 nm demonstrated a progressive enhancement in metabolic activity, suggesting elevated cellular proliferation. To evaluate effects on cell motility and invasive potential, we performed Transwell migration and Matrigel-coated invasion assays. H3F3B-overexpressing cells exhibited a 2- to 3-fold increase in the number of migrated and invaded cells compared with vector controls ($p < 0.01$; Fig. 5D–

E). High-resolution imaging and quantitative analysis indicated that H3F3B promotes reorganization of the cytoskeleton and facilitates extracellular matrix penetration, consistent with a pro-invasive phenotype. These data demonstrate that H3F3B functions as a potent oncogenic driver in LUAD, enhancing both proliferative capacity and invasive behavior, thereby establishing its mechanistic contribution to tumor progression in vitro.

3.6 Knockdown of H3F3B Suppresses LUAD Cell Proliferation, Migration, and Invasion

To determine the functional role of H3F3B in LUAD cells, we transfected A549 cells with siRNAs targeting H3F3B and verified knockdown efficiency. RT-qPCR and Western blot analyses confirmed a > 70% reduction in H3F3B mRNA and protein levels relative to scramble controls ($p < 0.01$; Fig. 6A–B**).** Cell proliferation assessed by CCK-8 assay demonstrated a significant decrease in growth rates over 96 hours in H3F3B-silenced cells, indicating impaired proliferative capacity ($p < 0.01$; Fig. 6C). In parallel, Transwell migration and Matrigel invasion assays showed a 50–60% reduction in migrated and invaded cells following H3F3B knockdown ($p < 0.01$; Fig. 6D–E), highlighting a critical role for H3F3B in promoting LUAD cell motility and invasive behavior.

3.7 H3F3B promotes LUAD progression through SEPTIN6 upregulation

To investigate potential downstream effectors of H3F3B in LUAD, we performed correlation analyses using our integrated single-cell transcriptomic dataset. SEPTIN6 emerged as the most strongly associated non-histone gene positively correlated with H3F3B expression (Spearman $r = 0.63$, FDR < 1e-72), suggesting a functional regulatory relationship. Clinical relevance was evaluated using Kaplan–Meier survival analysis. LUAD patients exhibiting high SEPTIN6 expression showed significantly reduced overall survival compared with patients with low SEPTIN6 expression ($p < 0.01$; Fig. 7A–B), indicating a prognostic role in tumor progression. Next, RT-qPCR and Western blot analyses of LUAD patient-derived tissues confirmed significant upregulation of SEPTIN6 in tumor samples relative to adjacent non-tumor tissues **(**Fig. 7C–D**)**. To validate causality, A549 cells were transfected with either H3F3B overexpression plasmids or H3F3B-targeting siRNAs. H3F3B overexpression significantly increased SEPTIN6 mRNA and protein levels, whereas H3F3B knockdown markedly reduced SEPTIN6 expression **(**Fig. 7E–G**)**, demonstrating that H3F3B directly modulates SEPTIN6 expression in LUAD cells. These results collectively indicate that H3F3B drives LUAD progression, at least in part, by upregulating SEPTIN6, thereby linking chromatin remodeling to cytoskeletal organization and enhancing proliferative, migratory, and invasive phenotypes. This regulatory axis highlights a mechanistic connection between epigenetic modulation and tumor cell dynamics, suggesting that H3F3B–SEPTIN6 signaling may serve as a potential therapeutic target in LUAD.

4. Discussion

Lung adenocarcinoma is characterized by profound cellular heterogeneity, which underlies its variable clinical outcomes and therapeutic responses. The current study employed integrative scRNA-seq of 665,761 epithelial cells from 878 lung-derived samples spanning non-cancer and NSCLC of clinical stages I–IV, enabling high-resolution dissection of epithelial diversity and the identification of malignant subpopulations. Our analyses reveal that secretory Club/AT2-like cells constitute the predominant malignant population in LUAD, while the histone variant H3F3B was prominently expressed within malignant epithelial populations and was associated with transcriptional programs related to proliferation and invasion. Functional experiments in A549 cells further demonstrated that H3F3B perturbation altered proliferative, migratory, and invasive phenotypes. H3F3B expression was also positively associated with SEPTIN6, and manipulation of H3F3B altered SEPTIN6 expression, supporting a potential regulatory relationship between these genes.

Dimensionality reduction and clustering resolved ten epithelial populations, including alveolar type 1 (AT1) and type 2 (AT2) cells, basal and ciliated cells, as well as malignant Secretory Club/AT2-like and Cycling Basal-like populations. Notably, malignant populations were confined to LUAD tissues, with Secretory Club/AT2-like cells representing nearly half of the malignant epithelial compartment. This observation aligns with prior lineage-tracing studies indicating that AT2 cells serve as the cell of origin for LUAD and that secretory differentiation programs contribute to tumor heterogeneity and stem-like features[18, 19]. The predominance of Secretory Club/AT2-like cells underscores their central role in sustaining malignant epithelial transcriptional programs. Differential gene expression analysis revealed 1,418 significantly dysregulated genes within Secretory Club/AT2-like cells, including 993 upregulated and 425 downregulated genes. Among the most significantly upregulated genes was H3F3B, implicating it as a potential driver of malignancy. Functional enrichment demonstrated that upregulated genes were associated with pathways involved in immune evasion, metabolic adaptation, and cell cycle regulation, including SemaA PAK-dependent axon repulsion, antigen processing and cross-presentation, interferon α/β signaling, platelet degranulation, and cell cycle checkpoint control. These observations resonate with findings from Chang et al., who reported that LUAD malignant cells co-opt immune modulation and proliferative signaling to enhance survival and expansion[20]. The concurrent engagement of immune-evasive and metabolic programs highlights the multifaceted role of Secretory Club/AT2-like cells in LUAD pathobiology. H3F3B emerged as a central hub in malignant epithelial networks, displaying significant upregulation across all LUAD stages, with a progressive increase from early to advanced disease. Network reconstruction indicated that H3F3B is extensively connected to histone variants (H4C3, H4C8, H4C11), chromatin remodeling factors, and cell cycle regulatory proteins, particularly within Secretory Club/AT2-like cells. This observation supports the model wherein histone variants serve as epigenetic modulators that orchestrate gene expression programs favoring proliferation and invasion [21]. The high H3F3B-centered network activity suggests that this histone variant functions not only in chromatin organization but also in integrating proliferative and invasive signaling within malignant subpopulations.

Correlation network analysis further identified SEPTIN6 as the top non-histone gene associated with H3F3B, establishing a putative regulatory axis linking chromatin remodeling to cytokinesis and cytoskeletal organization. Septins, including SEPTIN6, are essential for cytoskeletal dynamics, vesicle

trafficking, and cell division, and their dysregulation has been implicated in malignant progression across multiple cancers [22]. Our findings suggest that H3F3B overexpression may exert tumorigenic effects partially by regulating SEPTIN6, thereby coupling epigenetic control to structural cellular programs that drive migration and invasion. Experimental validation in LUAD patient tissues confirmed that H3F3B is markedly overexpressed in tumor cells relative to adjacent normal tissue, both at the mRNA and protein levels. Immunohistochemical analyses revealed strong nuclear localization of H3F3B in tumors, consistent with its role in chromatin modulation. Previous studies have reported similar overexpression patterns of H3F3B in solid tumors, including gliomas and melanoma, where it contributes to proliferative signaling and is associated with poor prognosis [23]. In LUAD, our findings extend these observations by demonstrating cell-type-specific overexpression within malignant Secretory Club/AT2-like populations, underscoring the contribution of epigenetic dysregulation to tumor heterogeneity.

Functional assays using the A549 LUAD cell line confirmed that H3F3B overexpression enhances proliferative, migratory, and invasive capacities. Overexpressing cells demonstrated significantly increased proliferation over multiple days, as measured by metabolic activity, and exhibited 2–3-fold higher migration and invasion in Transwell and Matrigel assays. Conversely, siRNA-mediated knockdown of H3F3B reduced proliferation and invasion by 50–60%, establishing a causal relationship between H3F3B expression and malignant phenotypes. These results are concordant with prior reports indicating that histone variants such as H3.3 modulate chromatin accessibility to activate proliferative and metastatic gene programs in lung cancer models[24, 25]. Importantly, the bidirectional modulation confirms that H3F3B is a potent driver of LUAD malignancy, not merely a correlative marker. SEPTIN6 emerged as a functionally relevant downstream target of H3F3B. Correlation analyses revealed that SEPTIN6 expression is strongly associated with H3F3B, and Kaplan–Meier survival analyses demonstrated that high SEPTIN6 expression predicts poorer overall survival in LUAD patients. In patient tissues, SEPTIN6 was significantly upregulated in tumors compared to adjacent normal tissues. Mechanistic experiments confirmed that H3F3B overexpression increases SEPTIN6 expression, while H3F3B knockdown decreases it. These data suggest that H3F3B promotes LUAD progression, at least in part, through transcriptional or post-transcriptional regulation of SEPTIN6. SEPTIN6 has previously been implicated in actin filament stabilization, epithelial–mesenchymal transition, and metastatic dissemination in lung cancer, supporting its role as a downstream effector of epigenetically driven tumor progression[26]. This H3F3B–SEPTIN6 axis mechanistically links chromatin remodeling with cytoskeletal reorganization, providing a molecular explanation for enhanced proliferation, migration, and invasion in malignant epithelial populations. The integration of scRNA-seq analysis with in vitro functional validation offers a comprehensive framework connecting transcriptional heterogeneity, epigenetic regulation, and functional tumor phenotypes. Secretory Club/AT2-like cells, as the dominant malignant epithelial subpopulation, exhibit transcriptional programs that integrate proliferative, immune-modulatory, and metabolic pathways. H3F3B operates as a central orchestrator of these programs, linking histone variant-mediated chromatin remodeling to downstream effectors such as SEPTIN6 that regulate cytoskeletal dynamics and invasive potential. This multi-layered evidence underscores the critical role of epigenetic drivers in shaping malignant phenotypes at the single-cell level, extending prior

bulk transcriptomic studies that could not resolve subpopulation-specific dynamics[27]. Mechanistically, our findings suggest that H3F3B contributes to LUAD aggressiveness through coordinated regulation of transcriptional and cytoskeletal programs. As a central hub within malignant epithelial networks, H3F3B was strongly associated with histone variants, chromatin regulatory factors, and cell-cycle-related genes, indicating a potential role in maintaining transcriptional states that favor tumor growth and progression. Functional analyses demonstrated that modulation of H3F3B expression significantly altered proliferative, migratory, and invasive capacities of LUAD cells, supporting its biological relevance. Notably, SEPTIN6 emerged as the strongest non-histone correlate of H3F3B and was consistently regulated following H3F3B overexpression or knockdown. Given the established role of septin family proteins in cytoskeletal organization, cell polarity, and migration, these findings suggest that H3F3B may promote malignant progression partly through activation of cytoskeleton-associated programs. This interpretation is consistent with evidence that epigenetic regulators and cytoskeletal remodeling pathways cooperate to facilitate tumor cell plasticity, invasion, and metastatic dissemination[28, 29]. From a translational perspective, H3F3B and SEPTIN6 may represent candidate molecular markers for further investigation in LUAD. However, the current evidence is insufficient to establish either molecule as a therapeutic target. Additional studies using independent LUAD models, mechanistic perturbation of SEPTIN6, and in vivo validation will be required to determine whether targeting this pathway has therapeutic potential. Interventions that disrupt H3F3B expression or block its ability to regulate SEPTIN6 could attenuate proliferative and invasive capabilities of LUAD cells. This strategy complements current efforts to target epigenetic regulators and cytoskeletal modulators in solid tumors, which have demonstrated preclinical efficacy in reducing tumor progression and metastasis[19, 22]. Furthermore, the identification of Secretory Club/AT2-like cells as a dominant malignant population provides a rationale for developing cell-type-specific interventions, potentially improving therapeutic precision and minimizing off-target effects.

Our study integrates single-cell transcriptomics, patient tissue validation, and mechanistic *in-vitro* assays to provide a detailed, cell-type-specific understanding of LUAD pathogenesis. The elucidation of the H3F3B–SEPTIN6 axis highlights a critical mechanistic connection between chromatin remodeling and cytoskeletal reorganization, advancing our understanding of how malignant epithelial subpopulations acquire enhanced proliferative and invasive capacities. These findings fill a crucial knowledge gap by defining the molecular drivers of LUAD at single-cell resolution and providing actionable targets for therapeutic development. From a precision-oncology perspective, the present findings highlight the potential utility of single-cell genomic profiling for identifying molecularly defined malignant epithelial states and candidate biomarkers that may be obscured in bulk tumor analyses. H3F3B and SEPTIN6 represent candidate markers associated with malignant epithelial phenotypes in LUAD; however, their clinical utility remains to be established. Future studies incorporating larger patient cohorts, independent validation datasets, treatment-response information, and longitudinal clinical data will be necessary to determine whether H3F3B–SEPTIN6-associated molecular states can contribute to patient stratification, prognostic assessment, or therapeutic decision-making.

Despite the comprehensive scope of this study, certain limitations warrant consideration. While the integration of 665,761 epithelial cells from 878 LUAD patient samples across multiple cohorts provided a robust atlas of malignant heterogeneity, single-cell transcriptomics captures only a snapshot of dynamic cellular states, and temporal plasticity or therapy-induced changes cannot be fully assessed. Additionally, in vitro validation was conducted solely in the A549 cell line, which, although widely used and mechanistically informative, may not capture the full spectrum of LUAD cellular behavior observed in diverse patient-derived models. Moreover, while our findings establish a functional regulatory axis between H3F3B and SEPTIN6, the precise molecular intermediates and chromatin remodeling events remain to be fully delineated. Finally, although multi-cohort integration and rigorous batch correction minimized inter-study variability, subtle differences in sample processing, sequencing platforms, and patient demographics could introduce residual bias. Importantly, these considerations highlight avenues for future research while underscoring the strength of our integrative approach, which combines high-resolution single-cell analysis with mechanistic in vitro validation, providing a solid framework for understanding LUAD progression and informing potential therapeutic targeting of the H3F3B–SEPTIN6 axis.

5. Conclusion

This study integrated large-scale single-cell transcriptomic analysis with patient tissue validation and functional experiments to characterize H3F3B in LUAD. H3F3B was enriched in malignant epithelial populations and was associated with transcriptional programs related to tumor progression. Experimental modulation of H3F3B altered proliferation, migration, and invasion in A549 cells and was accompanied by corresponding changes in SEPTIN6 expression. These findings support a potential H3F3B–SEPTIN6 regulatory relationship in LUAD. Further studies using additional LUAD models, larger patient cohorts, direct mechanistic assays, and SEPTIN6 rescue experiments are required to establish the molecular basis and clinical significance of this relationship.

Declarations

Ethical and Consent for publication: This study was conducted in accordance with the Declaration of Helsinki and approved by the Ethics Committee of Affiliated Haining Hospital of Jiaxing University (Approval ID: T20260130-X). Written informed consent for research participation and publication was obtained from all patients prior to sample collection.

Consent to publish: Written informed consent for publication was obtained from all patients included in this study.

Author contribution: XZ, LW, FY, CH, and JW made substantial contributions to the conception and design of the study, acquisition, analysis, and interpretation of data. XZ and LW contributed to drafting the manuscript, and all authors contributed to revising it critically for important intellectual content. All

authors approved the final version of the manuscript and agreed to be accountable for all aspects of the work.

Funding: This research did not receive any specific grant from funding agencies in the public, commercial or not-for-profit sectors.

Data availability: The single-cell RNA sequencing datasets analyzed in this study were obtained from publicly available repositories. The Chan et al. dataset (PMID: 34653364) was accessed through its CELLxGENE collection (Collection ID: 62e8f058-9c37-48bc-9200-e767f318a8ec). The Salcher et al. dataset (PMID: 36368318) was obtained from the European Genome–Phenome Archive (EGA) repository. The Sikkema et al. dataset (PMID: 37291214) was accessed through its CELLxGENE collection (Collection ID: 6f6d381a-7701-4781-935cdb10d30de293). The analysis code and processed data generated during the current study are available from the corresponding author upon reasonable request, subject to applicable data-use restrictions.

Clinical trial number: not applicable.

Conflict of Interest: The authors declare no competing interests.

References

1. Kim N, Kim HK, Lee K, Hong Y, Cho JH, Choi JW, Lee J-I, Suh Y-L, Ku BM, Eum HH, Choi S, Choi Y-L, Joung J-G, Park W-Y, Jung HA, Sun J-M, Lee S-H, Ahn JS, Park K, Ahn M-J, Lee H-O. Single-cell RNA sequencing demonstrates the molecular and cellular reprogramming of metastatic lung adenocarcinoma. Nat Commun. 2020;11:2285. https://doi.org/10.1038/s41467-020-16164-1.
2. Ortega-Batista A, Jaén-Alvarado Y, Moreno-Labrador D, Gómez N, García G, Guerrero EN. Single-Cell Sequencing: Genomic and Transcriptomic Approaches in Cancer Cell Biology. Int J Mol Sci. 2025;26:2074. https://doi.org/10.3390/ijms26052074.
3. Salcher S, Sturm G, Horvath L, Untergasser G, Kuempers C, Fotakis G, Panizzolo E, Martowicz A, Trebo M, Pall G, Gamerith G, Sykora M, Augustin F, Schmitz K, Finotello F, Rieder D, Perner S, Sopper S, Wolf D, Pircher A, Trajanoski Z. High-resolution single-cell atlas reveals diversity and plasticity of tissue-resident neutrophils in non-small cell lung cancer. Cancer Cell. 2022;40:1503–e15208. https://doi.org/10.1016/j.ccell.2022.10.008.
4. An H, An P. Single-cell and bulk RNA analysis identifies EMT-associated CAF signatures and prognostic model in lung adenocarcinoma. Discov Oncol. 2025;16:1106. https://doi.org/10.1007/s12672-025-02951-z.
5. Li M, Zhou B, Zheng C. An integrated bioinformatic analysis of bulk and single-cell sequencing clarifies immune microenvironment and metabolic profiles of lung adenocarcinoma to predict immunotherapy efficacy. Front Cell Dev Biol. 2023;11:1163314. https://doi.org/10.3389/fcell.2023.1163314.

6. Liu Y, Wang T, Zhou B, Zheng D. Robust integration of multiple single-cell RNA sequencing datasets using a single reference space. Nat Biotechnol. 2021;39:877–84. https://doi.org/10.1038/s41587-021-00859-x.
7. Park S-M, Choi E-Y, Bae M, Kim S, Park JB, Yoo H, Choi JK, Kim Y-J, Lee S-H, Kim I-H. Histone variant H3F3A promotes lung cancer cell migration through intronic regulation. Nat Commun. 2016;7:12914. https://doi.org/10.1038/ncomms12914.
8. Muhire BM, Booker MA, Tolstorukov MY. Non-neutral evolution of H3.3-encoding genes occurs without alterations in protein sequence. Sci Rep. 2019;9:8472. https://doi.org/10.1038/s41598-019-44800-4.
9. Okur V, Chen Z, Vossaert L, Peacock S, Rosenfeld J, Zhao L, Du H, Calamaro E, Gerard A, Zhao S, Kelsay J, Lahr A, Mighton C, Porter HM, Siemon A, Silver J, Svihovec S, Fong C-T, Grant CL, Lerner-Ellis J, Manickam K, Madan-Khetarpal S, McCandless SE, Morel CF, Schaefer GB, Berry-Kravis EM, Gates R, Gomez-Ospina N, Qiu G, Zhang TJ, Wu Z, Meng L, Liu P, Scott DA, Lupski JR, Eng CM, Wu N, Yuan B. De novo variants in H3-3A and H3-3B are associated with neurodevelopmental delay, dysmorphic features, and structural brain abnormalities. Npj Genom Med. 2021;6:104. https://doi.org/10.1038/s41525-021-00268-8.
10. Kwok KO, Wong V, Wei VWI, Wong SYS, Tang JW-T. Novel coronavirus (2019-nCoV) cases in Hong Kong and implications for further spread. J Infect. 2020;80:671–93. https://doi.org/10.1016/j.jinf.2020.02.002.
11. Chan JM, Quintanal-Villalonga Á, Gao VR, Xie Y, Allaj V, Chaudhary O, Masilionis I, Egger J, Chow A, Walle T, Mattar M, Yarlagadda DVK, Wang JL, Uddin F, Offin M, Ciampricotti M, Qeriqi B, Bahr A, de Stanchina E, Bhanot UK, Lai WV, Bott MJ, Jones DR, Ruiz A, Baine MK, Li Y, Rekhtman N, Poirier JT, Nawy T, Sen T, Mazutis L, Hollmann TJ, Pe'er D, Rudin CM. Signatures of plasticity, metastasis, and immunosuppression in an atlas of human small cell lung cancer. Cancer Cell. 2021;39:1479–e149618. https://doi.org/10.1016/j.ccell.2021.09.008.
12. Sikkema L, Ramírez-Suástegui C, Strobl DC, Gillett TE, Zappia L, Madissoon E, Markov NS, Zaragosi L-E, Ji Y, Ansari M, Arguel M-J, Apperloo L, Banchero M, Bécavin C, Berg M, Chichelnitskiy E, Chung M-I, Collin A, Gay ACA, Gote-Schniering J, Hooshiar Kashani B, Inecik K, Jain M, Kapellos TS, Kole TM, Leroy S, Mayr CH, Oliver AJ, von Papen M, Peter L, Taylor CJ, Walzthoeni T, Xu C, Bui LT, De Donno C, Dony L, Faiz A, Guo M, Gutierrez AJ, Heumos L, Huang N, Ibarra IL, Jackson ND, Kadur Lakshminarasimha Murthy P, Lotfollahi M, Tabib T, Talavera-López C, Travaglini KJ, Wilbrey-Clark A, Worlock KB, Yoshida M, Consortium LBN, van den Berge M, Bossé Y, Desai TJ, Eickelberg O, Kaminski N, Krasnow MA, Lafyatis R, Nikolic MZ, Powell JE, Rajagopal J, Rojas M, Rozenblatt-Rosen O, Seibold MA, Sheppard D, Shepherd DP, Sin DD, Timens W, Tsankov AM, Whitsett J, Xu Y, Banovich NE, Barbry P, Duong TE, Falk CS, Meyer KB, Kropski JA, Pe'er D, Schiller HB, Tata PR, Schultze JL, Teichmann SA, Misharin AV, Nawijn MC, Luecken MD, Theis FJ. An integrated cell atlas of the lung in health and disease. Nat Med. 2023;29:1563–77. https://doi.org/10.1038/s41591-023-02327-2.
13. Polański K, Young MD, Miao Z, Meyer KB, Teichmann SA, Park J-E. BBKNN: fast batch alignment of single cell transcriptomes. Bioinformatics. 2020;36:964–5.

https://doi.org/10.1093/bioinformatics/btz625.

14. Guo M, Morley MP, Jiang C, Wu Y, Li G, Du Y, Zhao S, Wagner A, Cakar AC, Kouril M, Jin K, Gaddis N, Kitzmiller JA, Stewart K, Basil MC, Lin SM, Ying Y, Babu A, Wikenheiser-Brokamp KA, Mun KS, Naren AP, Clair G, Adkins JN, Pryhuber GS, Misra RS, Aronow BJ, Tickle TL, Salomonis N, Sun X, Morrisey EE, Whitsett JA, Consortium NHLBILMAP, Xu Y. Guided construction of single cell reference for human and mouse lung. Nat Commun. 2023;14:4566. https://doi.org/10.1038/s41467-023-40173-5.
15. Robinson MD, McCarthy DJ, Smyth GK. edgeR: a Bioconductor package for differential expression analysis of digital gene expression data. Bioinformatics. 2010;26:139–40. https://doi.org/10.1093/bioinformatics/btp616.
16. Johnson WE, Li C, Rabinovic A. Adjusting batch effects in microarray expression data using empirical Bayes methods. Biostatistics. 2007;8:118–27. https://doi.org/10.1093/biostatistics/kxj037.
17. Yu G, Wang L-G, Han Y, He Q-Y. clusterProfiler: an R Package for Comparing Biological Themes Among Gene Clusters, OMICS: A. J Integr Biology. 2012;16:284–7. https://doi.org/10.1089/omi.2011.0118.
18. Chen Y, Toth R, Chocarro S, Weichenhan D, Hey J, Lutsik P, Sawall S, Stathopoulos GT, Plass C, Sotillo R. Club cells employ regeneration mechanisms during lung tumorigenesis. Nat Commun. 2022;13:4557. https://doi.org/10.1038/s41467-022-32052-2.
19. Wang Z, Wang Y, Chang M, Wang Y, Liu P, Wu J, Wang G, Tang X, Hui X, Liu P, Guo X, Xing B, Wang Y, Han Z, Ma W. Single-cell transcriptomic analyses provide insights into the cellular origins and drivers of brain metastasis from lung adenocarcinoma. Neuro Oncol. 2023;25:1262–74. https://doi.org/10.1093/neuonc/noad017.
20. Chang J, Lu J, Liu Q, Xiang T, Zhang S, Yi Y, Li D, Liu T, Liu Z, Chen X, Dong Z, Li C, Yi H, Yu S, Huang L, Qu F, Wang M, Wang D, Dong H, Cheng G, Zhu L, Li J, Li C, Wu P, Xie X, Teschendorff AE, Lin D, Wang X, Wu C. Single-cell multi-stage spatial evolutional map of esophageal carcinogenesis. Cancer Cell. 2025;43:380–e3977. https://doi.org/10.1016/j.ccell.2025.02.009.
21. Venkatesh S, Workman JL. Histone exchange, chromatin structure and the regulation of transcription. Nat Rev Mol Cell Biol. 2015;16:178–89. https://doi.org/10.1038/nrm3941.
22. Mostowy S, Cossart P. Septins: the fourth component of the cytoskeleton. Nat Rev Mol Cell Biol. 2012;13:183–94. https://doi.org/10.1038/nrm3284.
23. Kallappagoudar S, Yadav RK, Lowe BR, Partridge JF. Histone H3 mutations—a special role for H3.3 in tumorigenesis? Chromosoma. 2015;124:177–89. https://doi.org/10.1007/s00412-015-0510-4.
24. Lai PM, Gong X, Chan KM. Roles of Histone H2B, H3 and H4 Variants in Cancer Development and Prognosis. Int J Mol Sci. 2024;25:9699. https://doi.org/10.3390/ijms25179699.
25. Sester S, Wilms G, Ahlburg J, Babendreyer A, Becker W. Elevated expression levels of the protein kinase DYRK1B induce mesenchymal features in A549 lung cancer cells. BMC Cancer. 2024;24:1341. https://doi.org/10.1186/s12885-024-13057-0.

26. Li P, Yang X, Tang H, Zhou Z, Liu B. Cancer-associated fibroblasts-secreted lactate promotes RNA polymerase III subunit G-mediated epithelial–mesenchymal transition in non-small cell lung cancer by increasing m6A modification of zinc finger protein 384. J Cell Commun Signal. 2025;19:e70037. https://doi.org/10.1002/ccs3.70037.
27. Laughney AM, Hu J, Campbell NR, Bakhoum SF, Setty M, Lavallée V-P, Xie Y, Masilionis I, Carr AJ, Kottapalli S, Allaj V, Mattar M, Rekhtman N, Xavier JB, Mazutis L, Poirier JT, Rudin CM, Pe'er D. J. Massagué, Regenerative lineages and immune-mediated pruning in lung cancer metastasis, Nat Med 26 (2020) 259–269. https://doi.org/10.1038/s41591-019-0750-6
28. Chen JF, Yan Q. The roles of epigenetics in cancer progression and metastasis. Biochem J. 2021;478:3373–93. https://doi.org/10.1042/BCJ20210084.
29. Davies A, Zoubeidi A, Beltran H, Selth LA. The transcriptional and epigenetic landscape of cancer cell lineage plasticity. Cancer Discov. 2023;13:1771–88. https://doi.org/10.1158/2159-8290.CD-23-0225.

Figures

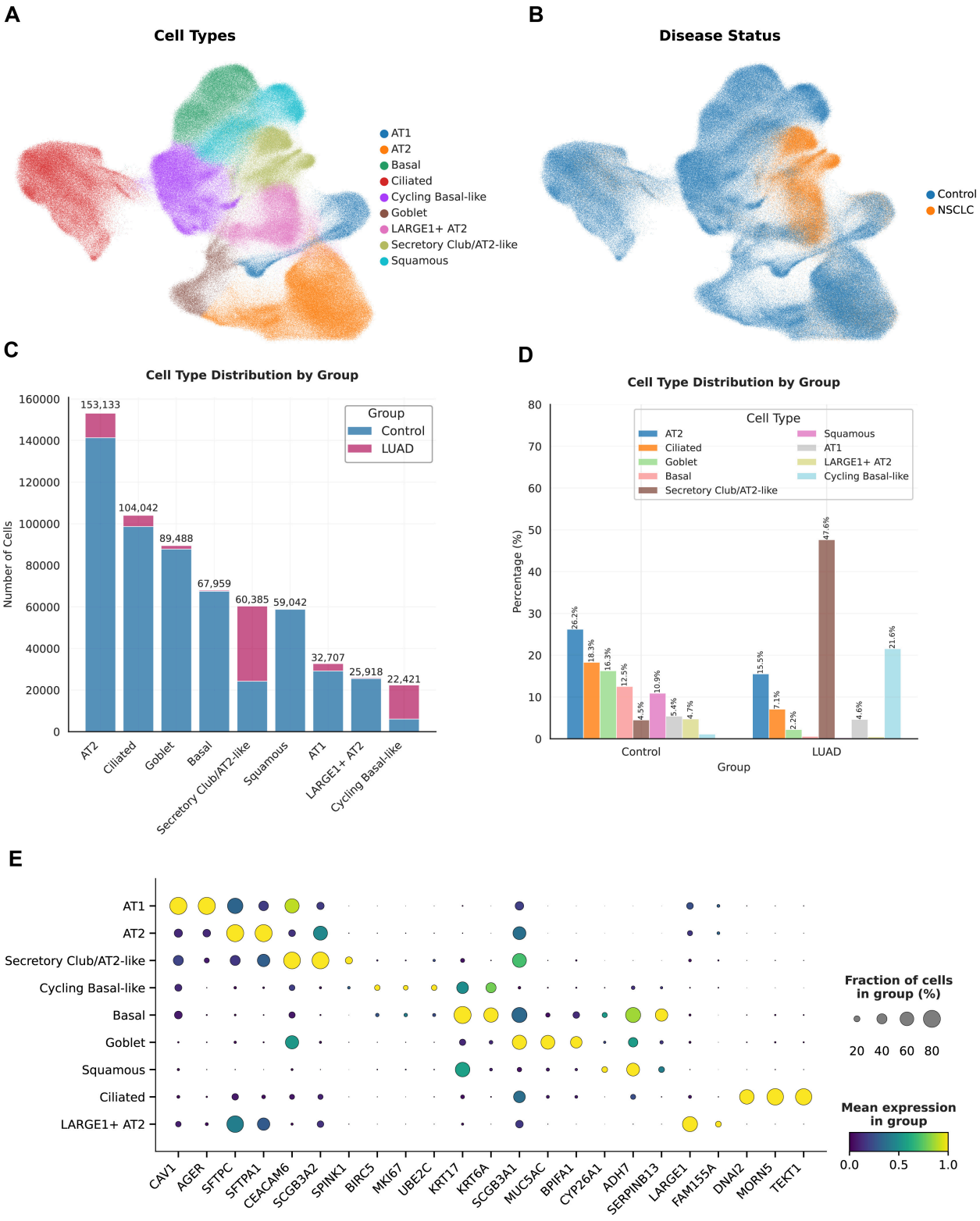


Figure 1

Single-Cell Transcriptomic Profiling Reveals Epithelial Cell Heterogeneity in Lung Adenocarcinoma

A. UMAP visualization colored by cell type annotation, revealing 10 distinct epithelial cell populations identified through marker-based classification. B. UMAP visualization colored by disease state (blue: control group, orange: non-small cell lung cancer), revealing disease-associated clustering patterns. C-D. Stacked

bar charts show number of cell type distribution across groups (C) and group percentage within each cell type (D), indicating shifts in cellular composition between control and LUAD samples. E. The dot plot matrix displays cell type-specific expression of representative marker genes, where dot size indicates the proportion of expressing cells and color represents the average expression level within each cell type.

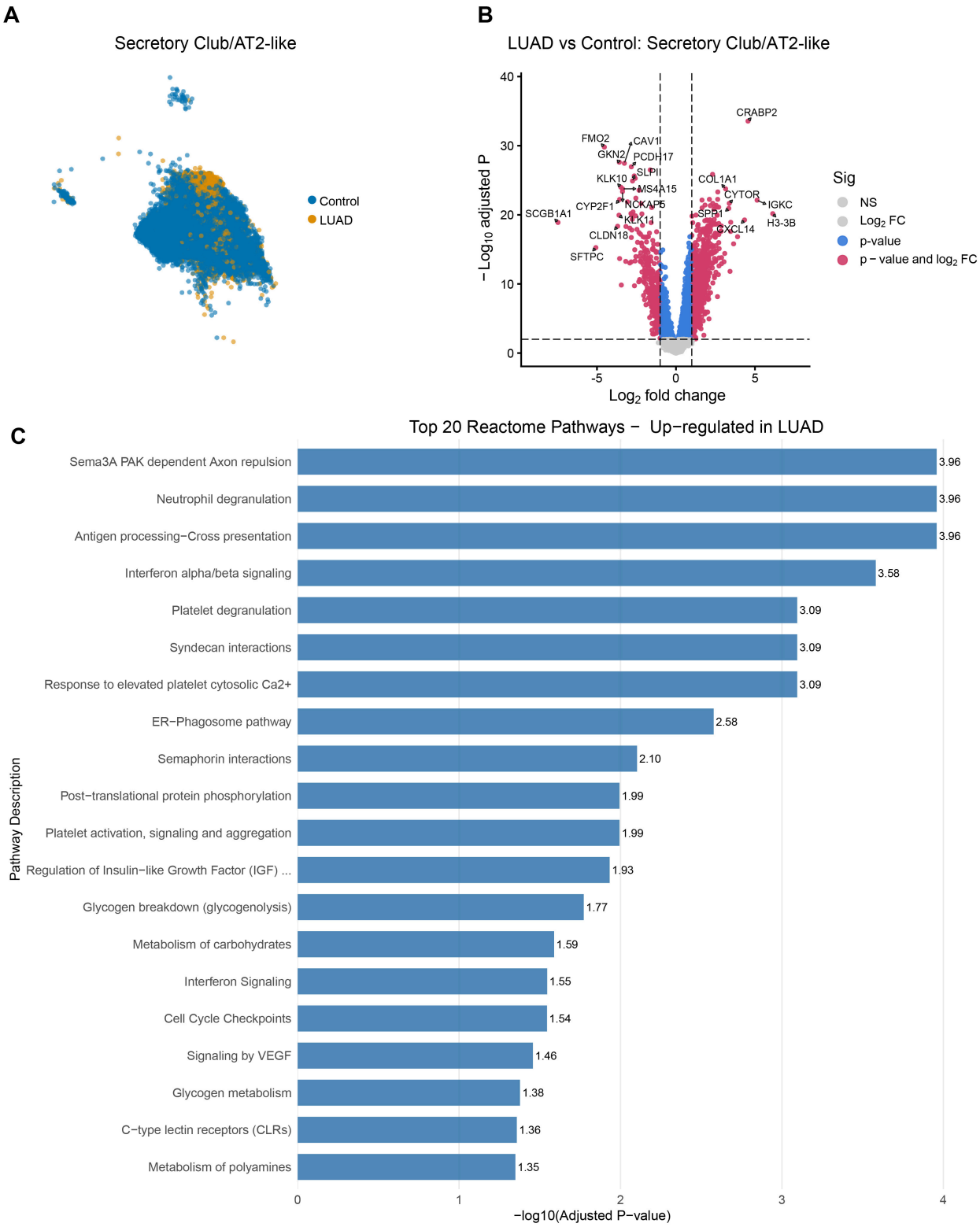


Figure 2

Differential Gene Expression and Pathway Enrichment in Secretory Club/AT2-like Cells.

A, UMAP visualization of Secretory Club/AT2-like cells colored according to disease status. B, Volcano plot showing differentially expressed genes between LUAD and control samples, using FDR <0.01 and |log2FC| >1 as significance criteria. C, Top 20 enriched Reactome pathways among genes upregulated in LUAD Secretory Club/AT2-like cells, ranked by adjusted P value.

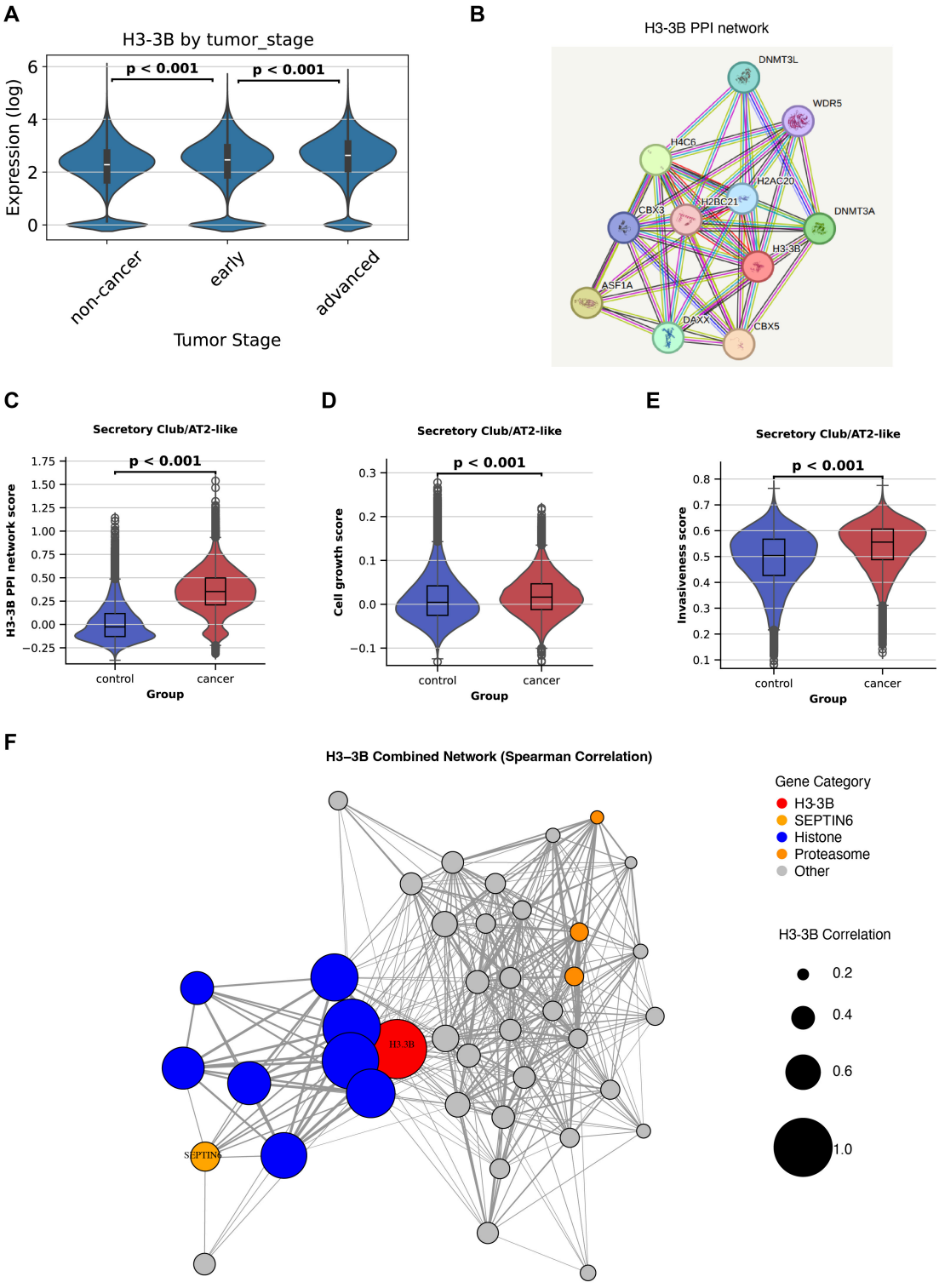


Figure 3

H3F3B Expression and Functional Network Characterization in LUAD

A, Violin plot showing H3F3B expression across non-cancer, early-stage, and advanced-stage samples. B, H3F3B-associated protein–protein interaction network. C, H3F3B PPI network score in Secretory Club/AT2-like cells between control and cancer groups. D, cell growth score in Secretory Club/AT2-like cells between control and cancer groups. E, invasiveness score in Secretory Club/AT2-like cells between control and cancer groups. F, combined Spearman correlation network showing genes associated with H3F3B.

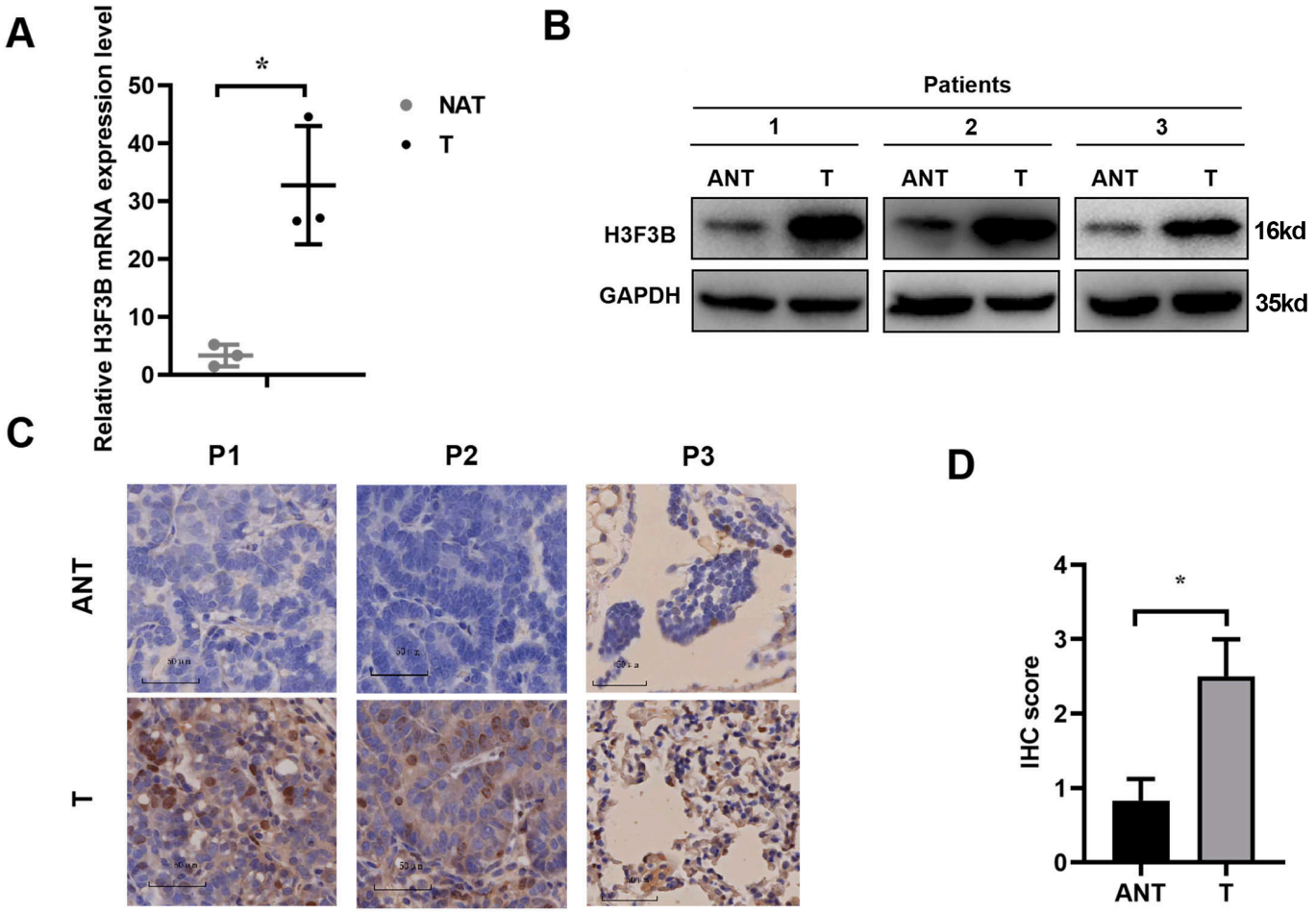


Figure 4

H3F3B Expression in Paired LUAD and Adjacent Tissue Specimens.

A, H3F3B mRNA expression measured by RT-qPCR in LUAD and paired adjacent tissue specimens. B, H3F3B protein expression assessed by Western blotting. C, representative immunohistochemical staining for H3F3B in paired adjacent and tumor tissues. Scale bar, 50 μm. D, quantitative immunohistochemical staining scores. Data were obtained from three paired patient specimens.

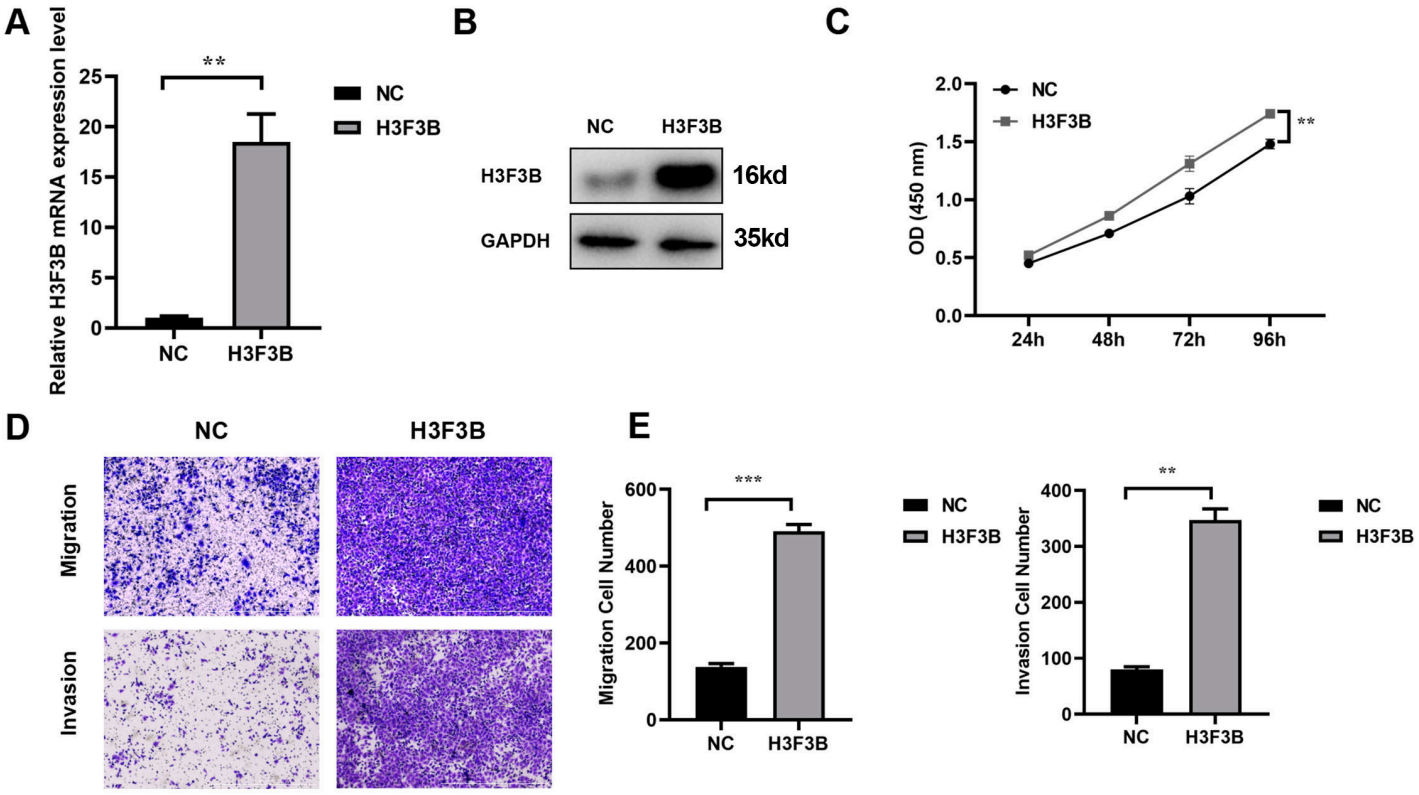


Figure 5

H3F3B Overexpression Enhances LUAD Cell Proliferation, Migration, and Invasion

*A, RT-qPCR showed increased mRNA expression of H3F3B in H3F3B-overexpressing A549 cells. (n=3, ** P < 0.01). B, Western blot showed increased protein expression of H3F3B in H3F3B-overexpressing A549 cells. C, CCK-8 assay was used to detect the ability of cell proliferation. (n=5, ** P < 0.01). D, Transwell experiment was used to measure the ability of cell migration and invasion in H3F3B-overexpressing A549 cells. E, The quantifiable data of D. (n=3, ** P < 0.01, *** P < 0.001)*

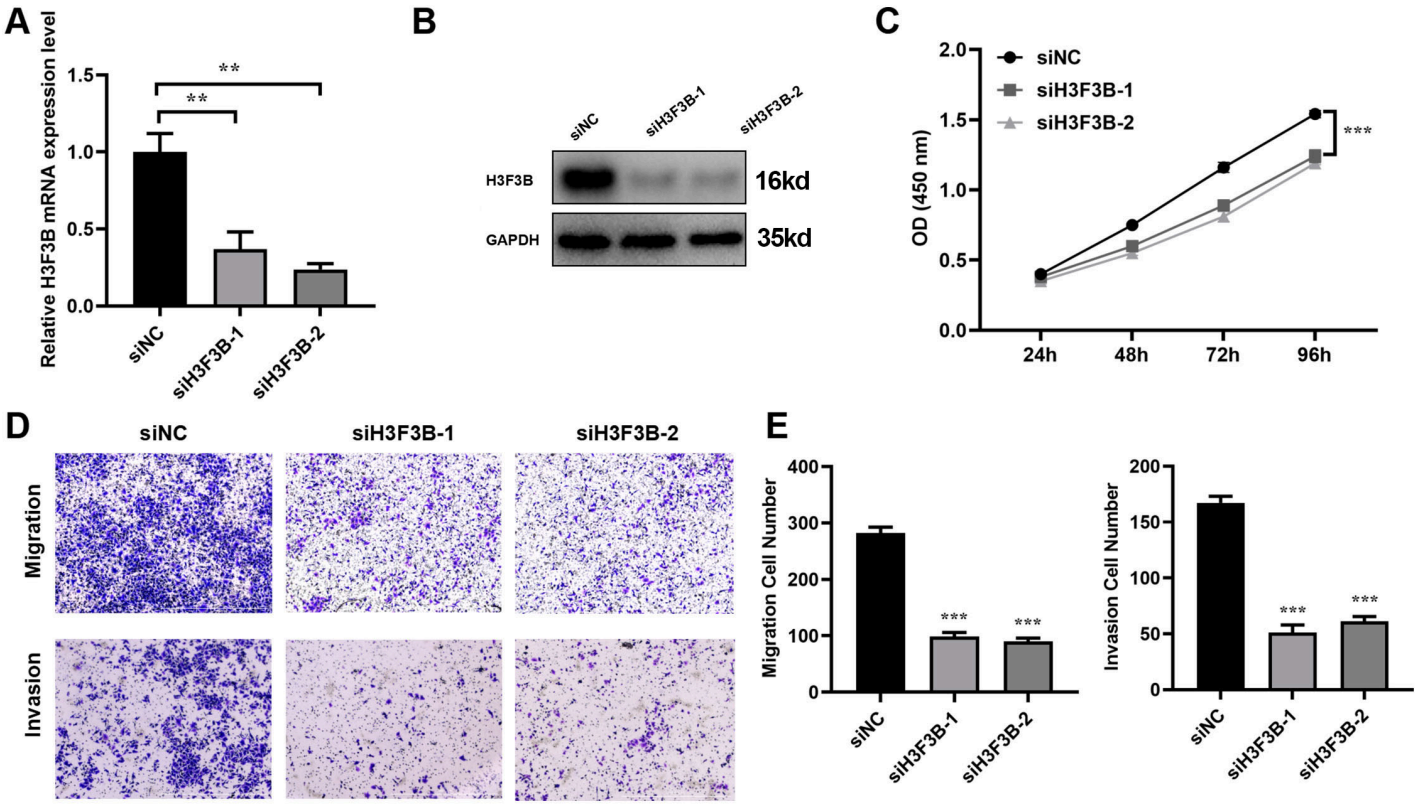


Figure 6

H3F3B Knockdown Suppresses Proliferation, Migration, and Invasion of A549 Cells.

A, RT-qPCR validation of H3F3B knockdown. B, Western blot validation of H3F3B knockdown. C, CCK-8 assay showing cell proliferation over 96 h. D, representative images of Transwell migration and Matrigel invasion assays. E, quantitative analysis of migrated and invaded cells. Data are presented as mean ± SD. The number of independent biological replicates is indicated in the figure.

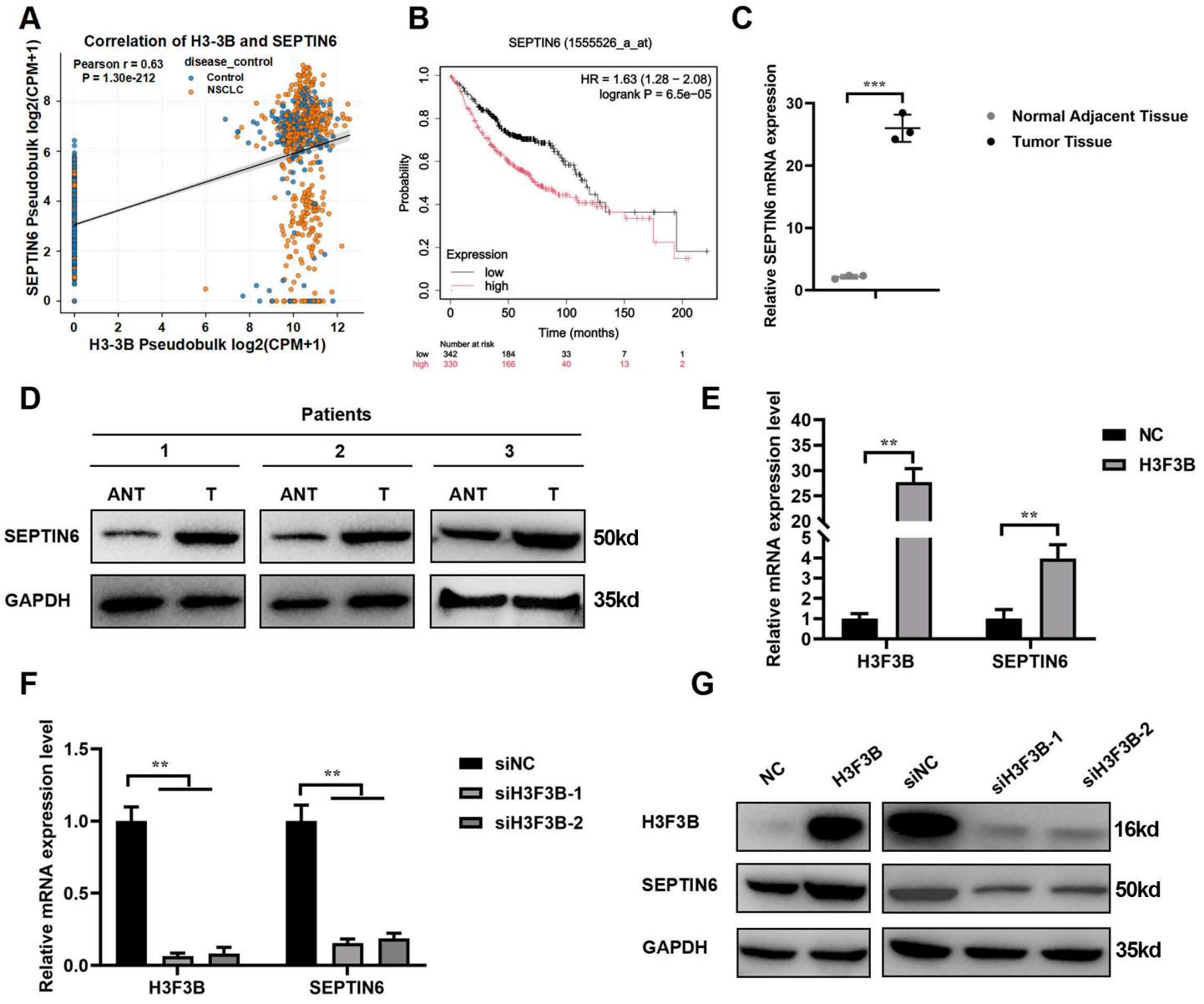


Figure 7

Association Between H3F3B and SEPTIN6 Expression in LUAD.

A, Correlation between H3F3B and SEPTIN6 expression in the integrated dataset. The correlation coefficient and statistical significance should correspond exactly to the final analysis output. B, Kaplan–Meier survival analysis according to SEPTIN6 expression. C, SEPTIN6 mRNA expression in LUAD and paired adjacent tissue specimens measured by RT-qPCR. D, SEPTIN6 protein expression in LUAD and paired adjacent tissue specimens measured by Western blotting. E–F, SEPTIN6 mRNA expression following H3F3B overexpression or knockdown in A549 cells. G, SEPTIN6 protein expression following H3F3B perturbation. Data are presented as mean ± SD.